Crossover of Varicose and Whipping Instabilities in Electrified Microjets

W. Yang, H. Duan, C. Li, and W. Deng
Department of Mechanical and Aerospace Engineering, University of Central Florida, Orlando, Florida 32816, USA
(Received 30 May 2013; published 5 February 2014)

In electrified liquid jets, varicose instability leads to jet breakup into droplets while whipping instability is responsible for jet stretching. We show that the coupling and relative importance of these two instabilities dictates the outcome for jet breakup. The codevelopment of transverse and radial perturbations lead to remarkable breakup modes linked to initial perturbation magnitude, perturbation wave numbers, and jet charge levels.

DOI: 10.1103/PhysRevLett.112.054501 PACS numbers: 47.65.-d, 47.20.Ma, 47.60.Kz

The breakup of liquid jets is ubiquitous with rich underpinning physics and widespread applications. The natural breakup of liquid jets originates from small ambient perturbations, which can grow exponentially until the amplitude as large as the jet radius is reached. For unelectrified inviscid jets, surface energy analysis [1,2] shows that only the axisymmetric perturbation is possibly unstable, and this mode is referred to as varicose instability. For electrified jets, the presence of a surface charge enables additional unstable modes, among which the most common one is the whipping (or kink) instability that bends and stretches the charged jet [3–9]. The whipping mode is responsible for the phenomena of electrospinning [10,11], which is a convenient approach for making nanofibers from a wide range of polymer solutions. A closer examination of the two instabilities suggests that due to mass conservation, the uneven jet stretching from whipping may translate into radial perturbations and trigger varicose instabilities. Although the varicose and whipping instabilities of electrified microjets have both been extensively studied separately, there is little attention paid to the combined effect of these two, which may lead to new jet breakup phenomena. Without a comprehensive physical picture of the relative importance of the coexisting varicose and whipping instabilities, the breakup of electrified jets can be neither fully understood nor well controlled.

In this Letter we show the phenomenology and a simplified linear model of electrified microjets undergoing both varicose and whipping instabilities. We show the perturbations of sweeping frequency lead to distinct jet breakups linked to perturbation wave numbers and jet charge levels. Interestingly, a bifurcation mode with clean breakup appears as the two instabilities cross over at the breakup point.

Experiments.—Figure 1(a) shows the schematic of the experimental setup. To generate electrified microjets, the liquid is fed through a stainless steel capillary (OD $= 300\,\mu$m and ID $= 150\,\mu$m) charged at ~2kV. Under the intense dc electric field, the liquid meniscus deforms into a Taylor cone [12], with a jet erupting from the tip of the cone. The liquids used in the experiment are pure ethanol. The jet diameter is controlled by varying the liquid flow rate from 1 to 16 ml/h, corresponding to the jet diameter from about 10 to 50 μm.

The transverse perturbation is introduced by the fringe electric field in a small gap (~200 μm) between two razor blades on the same plane. Each blade is mounted on an $x-y-z$ stage for precise gap adjustment and position alignment. The two blades, modeled as thin plates, are connected to a sinusoidal alternating current (ac) signal source. We choose to use thin plates instead of cylindrical rods or wires [13] because the plates essentially form an "extractor" electrode, allowing an intense dc component of the electric field to be established between the nozzle and the blades. At 15 mm below the blade electrodes is a collector electrode charged at voltage of -1 to -4 kV. The collector electrode has the dual function of sweeping

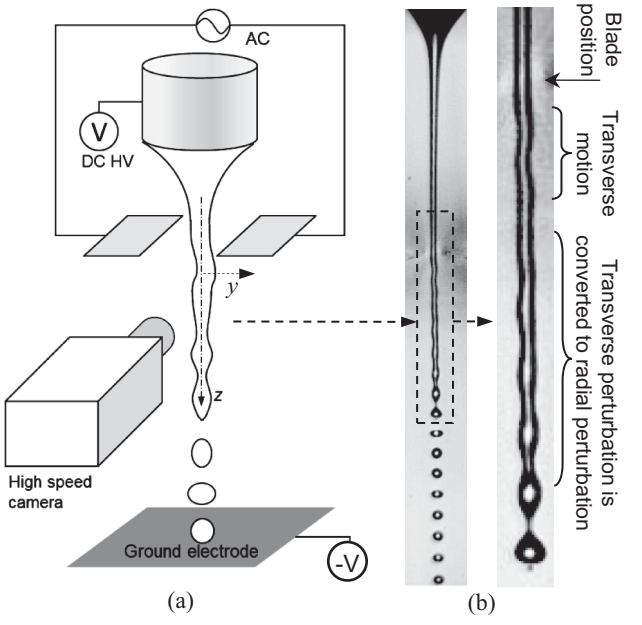

Fig. 1. Electrified microjet under transverse electrohydrodynamic perturbation. The jet radius is 10 μm.

 © 2014 American Physical Society

the charged droplets away from the blade electrode and adjusting the jet charge level (to be explained later). The ac signal has V_{pp} (peak-to-peak voltage) from 0 to 330 V with zero dc offset, and the virtual ground is the same as the dc power supplies. The horizontal electric field $E(z,t)$ at the symmetric plane of two large and thin plates can be solved using conformal mapping and the solution is

$$E(z,t) = E_0(z)\sin 2\pi f t,$$
$$E_0(z) = 2V_{pp}/[\pi a\sqrt{1+(z/a)^2}], \quad (1)$$

where $2a$ is the gap, and $z = 0$ corresponds to the position of the blade plane.

The ac frequency applied is from 10 to 200 kHz. The natural oscillation frequency of a liquid meniscus (Taylor cone in this case) can be estimated by $[\gamma/(\rho {R_n}^3)]^{1/2}$, where γ is the liquid-air interfacial tension, ρ is the liquid mass density, and R_n is the nozzle radius. For a typical nozzle diameter of 300 μm, the Taylor cone oscillation frequency is below 1 kHz, which is much less than the frequency range of the ac signal applied. Therefore, despite the fact that the blade electrodes are close to the nozzle, the setup can generate stable and reproducible electrified jets because the Taylor cone does not respond to the relatively high frequency ac signal.

The jet has surface charge density of $\sigma = I/(2\pi R v_j)$, where I is current carried by the jet, R is the unperturbed jet radius and v_j is the jet velocity. The dimensionless charge level Γ is defined as the ratio of electric stress to surface tension of the jet, i.e., $\Gamma = \sigma^2 R/\varepsilon_0\gamma$, with ε_0 being vacuum permittivity. Experimentally, Γ can be varied in two ways: either by changing the flow rate, or by changing the jet velocity. Note that σ is independent of the flow rate Q[14], while R scales with Q^α, where α is a scaling factor typically between 1/3 and 1/2. This suggests the charge level $\Gamma \propto Q^\alpha$. On the other hand, if Q is fixed, one can find that $\Gamma \propto v_j^{-2-\alpha}$, and the jet velocity v_j can be tuned by adjusting the driving field between the blades and the collector.

The experimental phenomena were recorded with a high speed camera (Phantom v12.1) and a long working distance microscope lens. A collimated LED light source is placed behind the jet and pointed to the camera to form the shadowgraph configuration.

Experimental results and discussion.—Figure 2 shows the typical experimental phenomena of electrified jets under transverse electrohydrodynamic (EHD) excitations at different wave number $x = 2\pi R f/v_j$. The image sequence suggests that the whipping dominates at small wave numbers while varicose is more prominent for larger wave numbers.

We can gain substantial insights from a simplified linear model without undertaking the complex nonlinear description of the problem. We first write a dispersion relationship for a charged jet [9]:

$$\omega_m{}^2 = \omega_R^2 x\frac{I_m'(x)}{I_m(x)}\left[(1-m^2-x^2) - \Gamma\left(1 + x\frac{K_m'(x)}{K_m(x)}\right)\right], \quad (2)$$

where ω_m is the instability growth rate at wave number x, $\omega_R = (\gamma/\rho R^3)^{1/2}$, $I_m(x)$, and $K_m(x)$ are modified Bessel functions of the first and second kind.

The phenomenology is consistent with the dispersion relationship [Eq. (2)], where the varicose growth rate is greater than the whipping growth rate for small x and the trend is reversed for large x. However, the growth rate alone does not paint the complete picture. The phenomenology should be determined by the combined effect of both growth rate and the initial perturbation. To that end, next we estimate the magnitude of initial transverse and radial

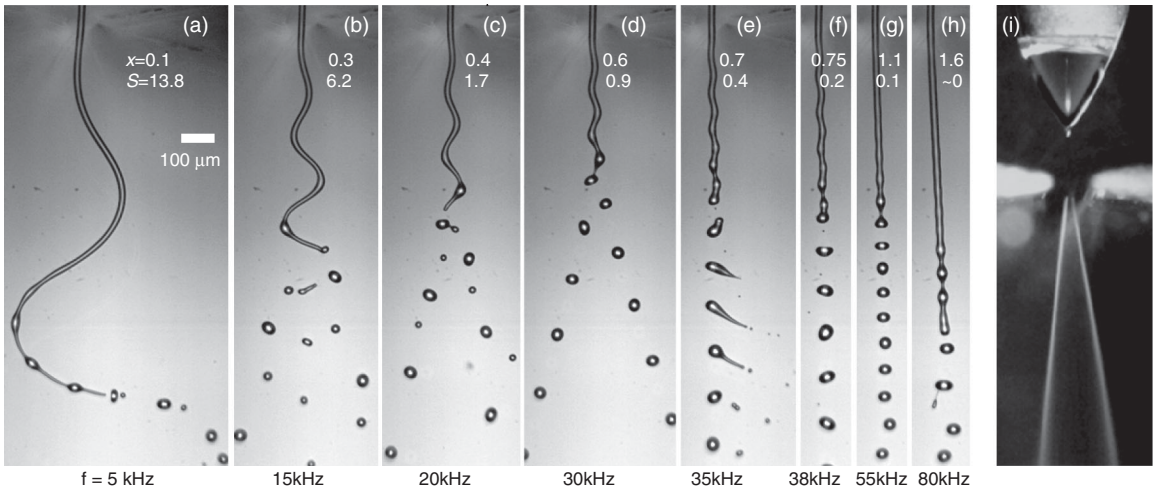

Fig. 2. Typical response of the electrified jet to external transverse perturbation introduced by the ac electric field between the narrow gap of two in-plane blade electrodes. $V_{pp} = 300$ V and $2a = 100\,\mu$m [15].

perturbations. We use the azimuthal number m to denote the perturbation mode, with $m = 0$, 1 being the axisymmetric (varicose) and transverse (whipping) perturbations, respectively. As the jet passes the blade electrodes, the horizontal stress acting on the jet is $E(z,t)\sigma$, and the jet will bend *transversely* with initial magnitude of δy during the first half cycle $1/(2f)$. The bending motion of the jet can be numerically solved if we only consider inertia and assume internal flows are negligible for small perturbations. These assumptions are proved to be reasonable, as decent agreement between δy obtained numerically and experimentally. Moreover, at sufficiently high frequency, within a half cycle $1/2f$, the jet only travels a short distance compared to a, i.e., $f > v_j/2a$. Then, $E(z,t) \approx E(z=0,t)$, which suggests that the dimensionless initial whipping perturbation is $\xi_1 = \delta y/\lambda = CV_{\mathrm{pp}}/(af)$, where C is a geometric correction factor of order 10^{-4} for the experimental setup in this work.

The radial perturbation can be estimated using mass conservation $\pi R^2 \mathrm{d}s + 2\pi R s \mathrm{d}R = 0$, where s is the stretched jet length over half wavelength $\lambda/2$, and $\mathrm{d}R$ can be interpreted as the radial perturbation. For sinusoidal curves with small magnitude, $\mathrm{d}s \approx \delta y^2/2\lambda$, and the dimensionless varicose perturbation is $\xi_0 = \mathrm{d}R/R = (\delta y/\lambda)^2/4 = {\xi_1}^2/4$.

At this point we can write η_m, the dimensionless radial $m = 0$ or transverse $(m = 1)$ perturbation as $\eta_m(t) = \xi_{\mathrm{m}} \exp(\omega_m t)$. Then the relative importance of the two instabilities can be quantified by the crossover ratio:

$$S = [\lambda \eta_1(t)]/[R\eta_0(t)], \tag{3}$$

Of particular interest of this ratio is the breakup point, at which the dimensionless radial perturbation grows into unity or $\eta_0(t_B) = 1$, where t_B is the time elapsed between the breakup point and the liquid mass first passes the EHD exciter. t_B is estimated by choosing the smaller value between excited breakup time $t_0 = -\ln(\xi_0)/\omega_0$ and natural breakup time $t_R \approx 35/\omega_R$ [16] (if the natural perturbation outgrows exited perturbation). Therefore, at the breakup point, the crossover ratio becomes

$$S = \lambda \eta_1(t_B)/R. \tag{4}$$

The S value indicates the relative importance of the whipping and varicose instabilities. Experimentally, λ can be obtained from the jet velocity and excitation frequency, while η_1 can be directly measured from images. We emphasize that because Eq. (4) is essentially based on a linear model, for small wave numbers the crossover ratio should be considered only qualitative.

In Fig. 2(a) $(x = 0.1)$, $S = 13.8 \gg 1$, indicating the whipping should dominate. Indeed, Fig. 2(a) clearly shows that whipping mode dictates the shape of the jet. The varicose mode appears to be superimposed on the whipping mode. As the wave number increases [Figs. 2(b) and 2(c)], the jet still exhibits primarily the whipping mode because S remains greater than unity. However, varicose mode plays an increasingly important role, leading to earlier jet breakup. Interestingly, near certain wave numbers, the crossover ratio S is close to 1 [Fig. 2(d)], and the importance of whipping and varicose modes is comparable, resulting in a unique whipping assisted bifurcation mode. The jet breaks up into two identical droplets within each excitation period without any satellite droplets. This phenomenon happens when the whipping mode has nonzero growth rate, and the 2nd harmonic of the applied perturbation is close to the Rayleigh frequency which has the maximum growth rate. When bifurcation is observed with the naked eye, the jet appears to split into two [Fig. 2(i)].

As the wavelength is further reduced, S becomes less than 1, whipping is suppressed, and the varicose instability dominates [Figs. 2(e)–2(g)]. Noticeably, in Fig. 2(e), the jet breaks up within each complete excitation period (instead of the half excitation period in the bifurcation mode) into dumb bell shaped liquid segments. When the liquid segment tries to regain spherical shape, the reduced surface area gives rise to surface charge density that exceeds the Rayleigh charge limit, in which electric stress overwhelms the surface tension. Consequently, the newly formed droplet would experience Coulombic fission [17,18], shedding smaller droplets to reduce the charge level of the main droplet below the Rayleigh limit [Fig. 2(e)].

In Fig. 2(g), the small value of S suggests that whipping instability virtually does not develop. The jet breakup is almost entirely governed by the varicose mode. At even higher wave number [Fig. 2(h)], the applied EHD excitation does not contribute to varicose instability, and the jet behaves similarly as a natural, unperturbed jet.

We can further map the phenomenology in the x–Γ diagram (Fig. 3) to take both charge levels and wave numbers into account. The distinct modes of jet response behavior are separated by boundaries set by the Rayleigh

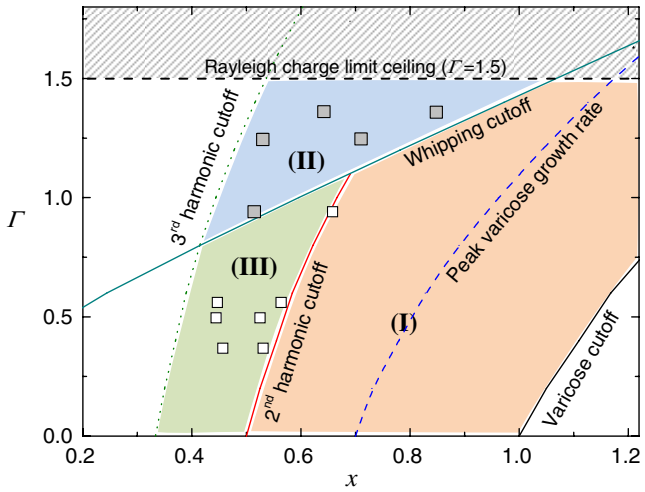

Fig. 3 (color online). Jet response phenomenon mapped in the x–Γ diagram. Scattered data points are experimental data.

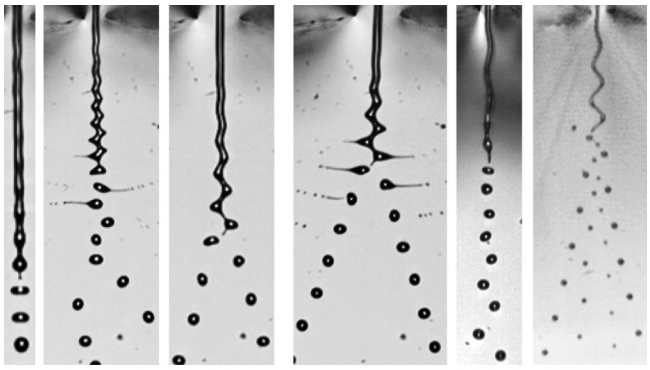

Fig. 4. Representative images for the $x-\Gamma$ diagram: (a) varicose mode, $Q = 16\,\mathrm{ml/h}, E_d = 2\,\mathrm{kV/cm}, x = 0.98, \Gamma = 0.99$; (b) overcharged varicose mode, $Q = 16\,\mathrm{ml/h}$, $E_d = 1\,\mathrm{kV/cm}$, $x = 1.21$, $\Gamma = 1.63$; (c) whipping assisted bifurcation, $Q = 16\,\mathrm{ml/h}$, $E_d = 2.5\,\mathrm{kV/cm}$, $x = 0.69$, $\Gamma = 1.32$; (d) overcharged whipping assisted bifurcation, $Q = 16\,\mathrm{ml/h}$, $E_d = 1.25\ \mathrm{kV/cm}$, $x = 0.69$, $\Gamma = 1.74$; (e) varicose assisted bifurcation, $Q = 14\ \mathrm{ml/h}$, $E_d = 2.5\ \mathrm{kV/cm}$, $x = 0.45, \Gamma = 0.56$; and (f) jet quadrufurcation as an effect of 4th harmonic of the Rayleigh frequency, $Q = 2\ \mathrm{ml/h}$, $E_d = 2.5\ \mathrm{kV/cm}$.

limit ceiling $\Gamma \geq 1.5$ and several cutoff curves obtained from the dispersion relationship. Here the "cutoff": refers to the zero growth rate of the corresponding instability, and below the cutoff curve, the corresponding instability will not grow. Specifically, these modes of jet response are

(i) *The varicose or Rayleigh mode.*—[zone I and Fig. 4(a)], which is at the proximity of the maximum growth rate of the varicose mode (dashed curve). Stronger perturbation (i.e., larger V_{pp}/a) will expand the area of the domains of the varicose mode. In principle, the domain is bound by the 2nd harmonic cutoff, whipping cutoff, and varicose cutoff curves. A submode can be identified as the overcharged varicose mode [Fig. 4(b)], which is above the Rayleigh limit ceiling, and generated droplets experience Coulombic fission.

(ii) *The whipping assisted bifurcation mode.*—[zone II and Fig. 4(c)], which is bound by the 3rd harmonic and whipping cutoff curves. In this domain, the whipping has nonzero growth rate and tears the jet in an alternating fashion that assists jet bifurcation. Again, above the Rayleigh limit ceiling, the generated droplets experience Coulombic fission [Fig. 4(d)]. In addition, stronger perturbation also will push the data points closer to the boundary of cutoff curves.

(iii) *The varicose assisted bifurcation mode.*—[zone III and Fig. 4(e)], which is bound by cutoff curves of the 2nd harmonics, 3rd harmonics, and whipping instabilities. In this mode, the jet charge levels are low and the jet wavy patterns from initial transverse perturbation will not be amplified because of the zero growth rate of whipping. It is the varicose instability that drives the wavy jet breakup. Bifurcation happens because the formed droplets are off from the center line alternatingly due to the initial wavy jet pattern. We note that jet bifurcation similar to the behavior in zone (iii) has been reported by Lin and Webb [19]. In [19], the liquid jet is charge neutral ($\Gamma = 0$), and the perturbation was introduced through the transverse vibration of a slender glass nozzle. Despite the different source of perturbation, the jet breakup behavior in [19] can still be categorized as varicose assisted bifurcation which falls into zone (iii) of the $x-\Gamma$ diagram.

At smaller wave numbers, phenomena corresponding to higher order harmonics of the Rayleigh mode can be identified. For example, Fig. 4(f) shows one such case. The jet appears to experience quadrufurcation, emitting four streams of droplets. It can be linked to the 4th harmonic of the Rayleigh mode. Here, during each complete transverse motion cycle, the 4th harmonic of the radial perturbation has a nonzero growth rate that breaks up the cycle into four droplets.

In summary, we have found and categorized different outcomes of breakup of electrified jets that undergo both varicose and whipping instabilities. The codevelopment of transverse and axisymmetric perturbations leads to remarkable jet breakup behavior attributable to initial perturbation magnitude, perturbation wave numbers, and jet surface charge levels. The experiment apparatus used in this work provides a simple and nonintrusive approach to systematically induce the whipping instability of the electrified microjets. The well-controlled triggering and codevelopment of the instabilities expands the possibilities of electrified jets breakup, and may spawn new ways of generating micro- or nanodroplets and controlled electrospinning.

We thank the National Science Foundation (Grants No. CMMI 1301099 and No. CMMI 1335295) for financial support.

[1] J. Plateau, Acad. Sci. Bruxelles Mem. **23**, 5 (1849).
[2] Lord, J. W. S. Rayleigh, Proc. London Math Soc. **10**, 4 (1879).
[3] J. B. Keller, S. I. Rubinow, and Y. O. Tu, Phys. Fluids **16**, 2052 (1973).
[4] D. P. Wang, J. Fluid Mech. **34**, 299 (1968).
[5] M.-C. Yuen, J. Fluid Mech. **33**, 151 (1968).
[6] A. H. Nayfeh, Phys. Fluids **13**, 841 (1970).
[7] P. Lafrance, Phys. Fluids **18**, 428 (1975).
[8] K. C. Chaudhary and L. G. Redekopp, J. Fluid Mech. **96**, 257 (1980).
[9] A. L. Huebner and H. N. Chu, J. Fluid Mech. **49**, 361 (1971).
[10] M. Hohman, M. Shin, G. Rutledge, and M. Brenner, Phys. Fluids **13**, 2201 (2001).
[11] S. V. Fridrikh, J. H. Yu, M. P. Brenner, and G. C. Rutledge, Phys. Rev. Lett. **90**, 144502 (2003).
[12] M. Cloupeau and B. Prunet-Foch, J. Electrost. **22**, 135 (1989).

[13] M. Crowley, Phys. Fluids **8**, 1668 (1965).
[14] A. M. Gañán-Calvo, J. Aerosol Sci. **30**, 863 (1999).
[15] See Supplemental Material at http://link.aps.org/supplemental/10.1103/PhysRevLett.112.054501 for videos of typical jet response behavior with setup in Fig. 2.
[16] S. P. Lin and R. D. Reitz, Annu. Rev. Fluid Mech. **30**, 85 (1998).
[17] A. Gomez and K. Tang, Phys. Fluids **6**, 404 (1994).
[18] D. Duft, T. Achtzehn, R. Müller, B. A. Huber, and T. Leisner, Nature (London) **421**, 128 (2003).
[19] S. P. Lin and R. D. Webb, Phys. Fluids **6**, 2671 (1994).